Journal of Solid State Electrochemistry (2019) 23:1351–1358
https://doi.org/10.1007/s10008-019-04216-6

ORIGINAL PAPER

# A novel method for the modification of $LiNi_{0.8}Co_{0.15}Al_{0.05}O_2$ with high cycle stability and low pH

**Chunhui Cao[1,2] · Jian Zhang[1] · Xiaohua Xie[1] · Baojia Xia[1]**

Received: 12 June 2018 / Revised: 23 December 2018 / Accepted: 11 February 2019 / Published online: 9 March 2019


## Abstract

Ni-rich cathode materials have high specific capacity and low cost, but they also have several drawbacks, such as high pH and poor cycle stability. In this paper, a simple dry-coat method using $MnCO_3$ was adopted to improve the performance of $LiNi_{0.8}Co_{0.15}Al_{0.05}O_2$ (NCA), which is the first report of its kind. The modified NCA showed a capacity of 193 mAh $g^{-1}$ and capacity retention of 98.9% at 1 °C rate after 100 cycles, compared to the corresponding values (195 mAh $g^{-1}$ and 94.0%) for the pristine NCA. The pH was reduced from 12.19 to 11.69. Moreover, the storage performance in air and thermal stability in the delithiated state were also improved.

**Keywords** $MnCO_3$ · $LiNi_{0.8}Co_{0.15}Al_{0.05}O_2$ · Dry-coat · Cycle stability · pH

## Introduction

With the rapid development of electric vehicles, Ni-rich cathode materials are attracting increasing attention due to their high specific capacity and low cost per kWh. Among these materials, Co and Al co-substituted $LiNi_{0.8}Co_{0.15}Al_{0.05}O_2$ (NCA) is one of the most promising materials with excellent electrochemical properties and thermal stability. However, there are some intrinsic problems associated with these materials, such as poor storage performance in air and fast capacity degradation during cycling, which are closely related to the surface properties of Ni-rich cathode materials.

It is generally accepted [1–4] that a NiO-like phase is formed on the surface of particles due to the reduction of $Ni^{3+}$ in cathode, which is responsible for the increase in impedance and capacity fading during long cycling. On the other hand, some residual lithium compounds in the form of LiOH or $Li_2CO_3$ [5, 6] are usually present on the surface of Ni-rich cathode materials, resulting in high pH. These compounds may cause swelling of the battery during cycling and gelation of the slurry during the electrode manufacturing process. It has been reported that Ni-rich cathode materials adsorb trace amounts of $H_2O$ and $CO_2$ and form a layer of LiOH and $Li_2CO_3$ on the surface when exposed to air [7, 8], accompanied by the reduction of $Ni^{3+}$ to $Ni^{2+}$ [9, 10] and cation mixing [11, 12] in the crystal structure.

Much efforts have been made to reduce the content of residual lithium and improve the surface stability of Ni-rich cathode materials. Washing is the most direct way to remove the residual lithium. However, the electrochemical performance is affected by water washing due to the phase transformation on the surface [13, 14]. Additionally, the wastewater is also a major problem for large-scale production [15]. Ethanol washing is considered effective to reduce

✉ Jian Zhang
zjskycn@163.com

Chunhui Cao
caochunhui@live.com

Xiaohua Xie
xiaohuaxie@126.com

Baojia Xia
xiabj@mail.sim.ac.cn

[1] Research Center for New Energy Technology, Shanghai Institute of Microsystem and Information Technology, Shanghai, China

[2] University of Chinese Academy of Sciences, Beijing, China

the content of residual lithium without significantly deteriorating the electrochemical properties. Nevertheless, ethanol washing is not an efficient method due to the low solubility of LiOH and $Li_2CO_3$ in ethanol [11, 16]. Another approach is to consume the residual lithium by reacting it with other substances. Surface fluorination can convert the residual lithium into stable LiF without sacrificing the electrochemical performance [17]. However, the fluorination process is always accompanied by the production of HF, which can severely damage manufacturing equipment [18].

Layered $Li_2MnO_3$ can be well integrated with layered $LiMO_2$ to form a homogeneous layered-structure composite, such as in lithium-rich cathodes [19]. It has been reported that Mn-surface-modified NCA showed excellent cycle stability and storage performance [20, 21]. Yang et al. [22] and Zhang et al. [23] adopted a precipitation method to coat $Li_2MnO_3$ on the surface of Ni-rich cathode. The cycle stability (up to 4.5 V vs. $Li/Li^+$, similar thereafter) and thermal stability of the $Li_2MnO_3$-coated materials were improved significantly, which was attributed to the suppression of the reaction between cathode and electrolyte [24].

However, all the above $Li_2MnO_3$-coating methods were implemented before the synthesis of Ni-rich cathode since post-heating of Ni-rich cathode at high temperature would increase the cation mixing and residual lithium [25]. In this work, an effective method was developed to coat $Li_2MnO_3$ on the surface of NCA at low temperature. The cycle stability and storage performance in air were greatly enhanced for the coated NCA cathode.

## Experimental

### Synthesis

The NCA powder was prepared by mixing $Ni_{0.8}Co_{0.15}Al_{0.05}(OH)_2$ (Henan Kelong New Energy Co., Ltd, Xinxiang) and $LiOH{\cdot}H_2O$ (Tianqi Lithium, 99.0%) with a molar ratio of 1:1.02 and sintering at 750 °C for 12 h under flowing oxygen. Then, 200 g NCA and 4.3 g $MnCO_3$ (Jinhuitaiya, Tianjin, 200 nm) were thoroughly mixed by ball milling and annealed at 300, 400, and 500 °C for 4 h. The resulting products were denoted as NCA-300, NCA-400, and NCA-500, respectively. The pristine NCA was denoted as NCA-pristine. The added $MnCO_3$ was expected to form $Li_2MnO_3$ by reacting with residual LiOH in NCA.

### Characterization

X-ray diffraction (XRD) patterns were measured using a Rigaku D/max-2200PCX diffractometer with Cu-K$\alpha$ radiation at 4 ° $min^{-1}$ between the 2$\theta$ range of 15 and 70°.

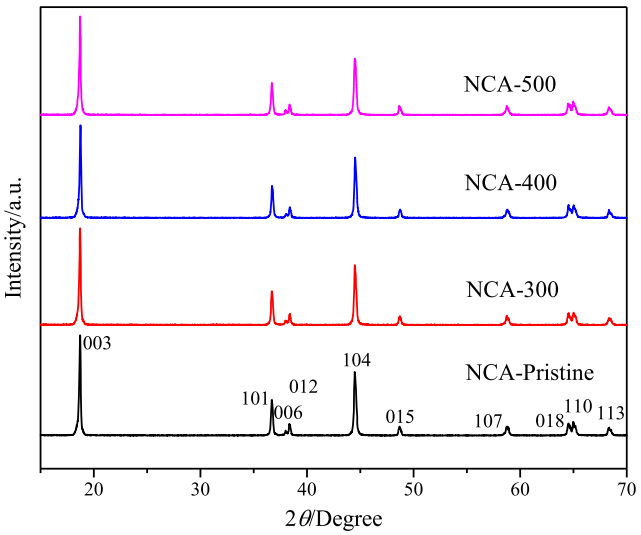


**Fig. 1** XRD patterns for pristine NCA and coated NCA at 4° $min^{-1}$ between 15 and 70°

The scanning step size was 0.05°. The morphology of the samples was observed using scanning electron microscopy (SEM, Hitachi, S4700). High-resolution transmission electron microscopy (HRTEM) images were obtained using a FEI Talos F200X system.

Samples for TG/DTA (STA4493F3, NETZSCH) measurement were prepared by the following method: cathode containing NCA was charged to 4.3V at 0.1 °C rate (20 mA $g^{-1}$). After charging, the electrode was removed from the cells in a glove box (Superstar 1220/750, Mikrouna) filled with argon gas and washed in dimethyl carbonate (DMC, Zhuhai Saiwei). After drying, the charged NCA material was collected and placed in a sample pan. It was heated to 350 °C in argon atmosphere at the rate of 5 °C $min^{-1}$.

The total lithium content, represented by the ratio of Li to (NiCoAl), was determined by inductively coupled plasma-atomic emission spectrometry (ICP-AES, IRIS Advantage, Thermal Scientific). The pH was measured by pH meter (PHS-3E, LEICI) at 25(±2)°C and the ratio of NCA to water was 1:10 by weight.

The samples for storage tests were stored in air at 25(±2)°C with humidity of 80% and weighed daily using an electronic balance with 0.1 mg accuracy.

**Table 1** The cell parameters of pristine NCA and coated NCA

| | $a$ (Å) | $c$ (Å) | $c/a$ | $V$ (Å$^3$) | $I_{003}/I_{104}$ |
|---|---|---|---|---|---|
| NCA-pristine | 2.868 | 14.20 | 4.952 | 101.15 | 1.30 |
| NCA-300 | 2.868 | 14.20 | 4.952 | 101.12 | 1.28 |
| NCA-400 | 2.867 | 14.19 | 4.949 | 100.96 | 1.26 |
| NCA-500 | 2.868 | 14.19 | 4.949 | 101.09 | 1.24 |

## Electrochemical characterization

Electrochemical behaviors of the as-prepared materials during charge/discharge cycles were examined using a 2025-coin cell with lithium foil(Tianjin Zhongneng) as the negative electrode. To prepare the positive electrode, the NCA active material, Super-P(Tianjin Yiborui), and polyvinylidene fluoride binder(PVDF, Arkema) were homogeneously mixed in N-methyl pyrrolidone (NMP, Nanjing Jinlong) with a weight ratio of 85:9:6. Then, the resulting slurry was spread on an aluminum current collector and dried at 110 °C to remove NMP solvent. The electrodes were punched into disks of 14 mm diameter. Celgard 2400 microporous polypropylene membrane was used as the separator. The electrolyte(Shandong Hairong) was 1 M $LiPF_6$ in a 1:1:1 mixture of ethylene carbonate(EC), DMC, and ethyl methyl carbonate (EMC). The cells were assembled in the glove box.

Galvanostatic charge/discharge tests were performed with a Neware battery testing system (CT-3008W, NEWARE) within the potential range of 2.75–4.3 V. The charge process was set with constant current and constant voltage(CC-CV), where the cut-off voltage was 4.3 V and cut-off current was 0.1 °C. The current density of working

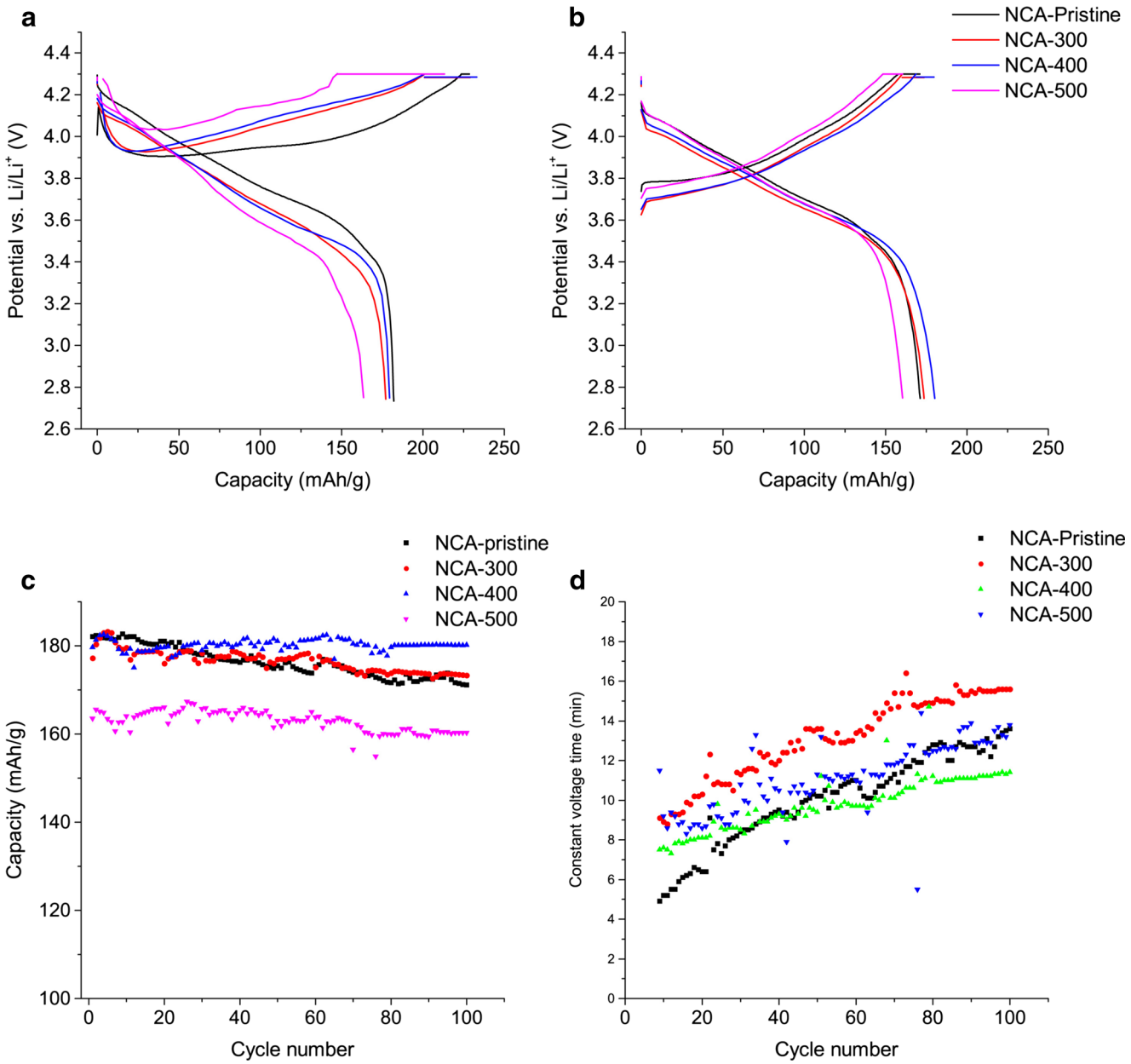


**Fig. 2** Performances for pristine and coated NCA **a** first charge-discharge curve at 1 °C; **b** 100th charge-discharge curve at 1 °C; **c** capacity retention; **d** constant voltage time at each cycle

electrodes at 1 °C was 200 mA $g^{-1}$. Cyclic voltammetry (CV) was performed after first charge/discharge at a scan rate of 0.1 mV $s^{-1}$ and electrochemical impedance spectroscopy (EIS) was performed before cycling between 100 k and 0.05 Hz with a 10-mV amplitude (Metrohm Autolab PGSTAT204). All tests were performed at 25(±2)°C.

## Results and discussion

### Structure characterization

Figure 1 shows the XRD patterns of the pristine and $MnCO_3$-modified NCA. All peaks were consistent with the layered $\alpha$-$NaFeO_2$ structure of space group $R\bar{3}m$. The lattice constants $a$ and $c$ were calculated from Rietveld analysis and are listed in Table 1. The $I_{003}/I_{104}$ ratio is used as an indicator of cation mixing. A low $I_{003}/I_{104}$ value indicates a high degree of cation mixing, due to occupancy of $Ni^{2+}$ in the lithium layer. The pristine sample showed the highest $I_{003}/I_{104}$ ratio of 1.30, indicating that this sample had the lowest amount of cation mixing. The low cation mixing means less $Ni^{2+}$; therefore, the sample showed high reversible capacity [24]. As the heat treatment temperature increased, the $I_{003}/I_{104}$ ratio decreased gradually, indicating that the heat treatment induced the migration of $Ni^{2+}$ from transition metal layer to the lithium layer. This migration will hinder the diffusion of $Li^+$ and hence decrease the specific capacity of NCA.

### Electrochemical performance

The electrochemical tests showed that the capacities for NCA-pristine, NCA-300, NCA-400, and NCA-500 were 195, 193, 193, and 182 mAh $g^{-1}$, respectively, for the first

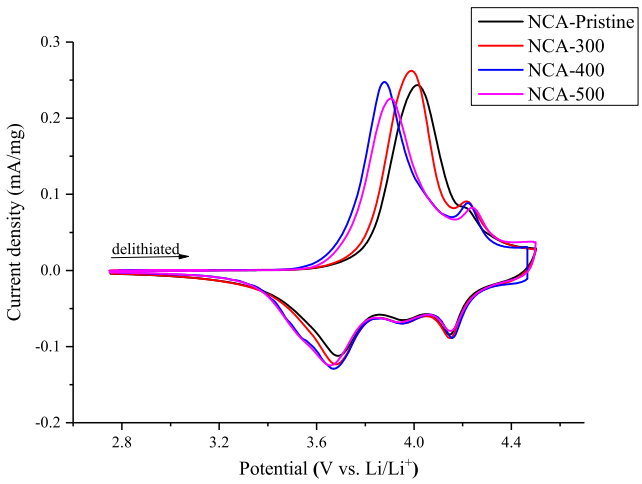


**Fig. 3** Cyclic voltammetry curves for pristine and coated NCA at a scan rate of 0.1 $mVs^{-1}$

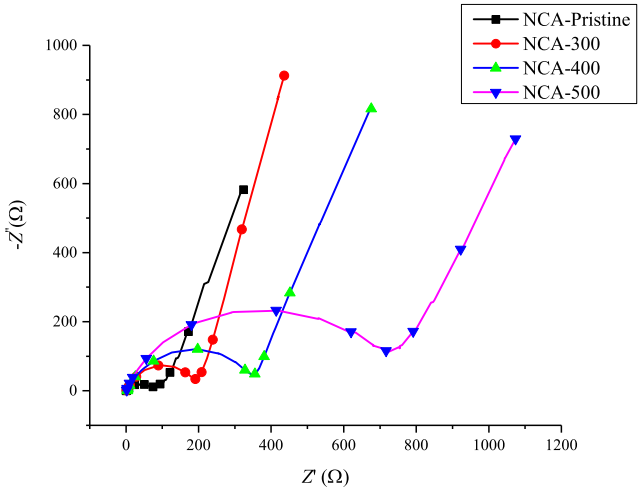


**Fig. 4** Electrochemical impedance spectroscopy for pristine and coated NCA

cycle at 0.1 °C between 2.75–4.3 V. The slight decrease in capacity for NCA-300 and NCA-400 was due to the introduction of inactive $Li_2MnO_3$. The significant decrease in capacity for NCA-500 was the result of increase in cation mixing and impedance, which was consistent with the XRD results. Figure 2a shows the initial charge-discharge curve of coin cells at 1 °C. It was evident that the charge plateau became higher and the discharge plateau became lower as the treatment temperature increased. This indicated that surface polarization increased, which may be caused by the presence of $Li_2MnO_3$ on the coated surface. After 100 cycles (Fig. 2b), the cell with NCA-400 cathode showed the lowest increase in polarization and the highest capacity.

The cycle stability of NCA-400 was best with a capacity retention of 98.9% after 100 cycles, compared to 94.0% for

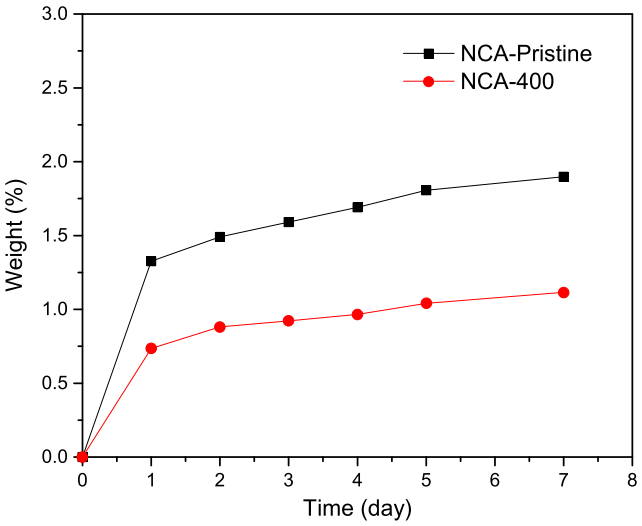


**Fig. 5** Weight gain for samples stored in air at 25(±2) °C with humidity of 80%

**Table 2** Lithium content and pH of pristine NCA and coated NCA

| | NCA-pristine | NCA-300 | NCA-400 | NCA-500 |
|---|---|---|---|---|
| Total Li | 1.004 | 1.000 | 1.001 | 0.999 |
| pH | 12.19 | 11.84 | 11.69 | 11.70 |

NCA-pristine (Fig. 2c). The improved cycle performance could be attributed to the modification of solid-liquid interface between NCA and electrolyte.

Since the charging method was CC-CV, constant voltage time can represent the degree of polarization to a certain extent. If the impedance is large, the initial potential for NCA when the voltage reaches 4.3 V would be low due to the polarization. Therefore, the time from initial potential to 4.3 V is long, which is the constant voltage time. It is worth mentioning that this parameter has not been reported in other papers but it clearly showed the impedance increase during cycle.

Figure 2d shows that the increase in constant voltage time of NCA-400 during cycling was smaller than that of the other three samples. This also confirmed the suppression of side reactions for NCA-400 and the solid-liquid interface modification. The capacity fading during cycling is due to the formation of inactive NiO-like phase [26], which is generated by the side reaction with electrolyte. The introduced $Li_2MnO_3$ improved the surface properties between cathode and electrolyte and thus enhanced the cycle stability significantly.

Cyclic voltammetry results (Fig. 3) showed that the oxidation peak gradually shifted towards the positive potential with the increase in heating temperature, which indicated increased polarization. Ohzuku [27] reported that $Li_{1-x}NiO_2$ undergone three transitions between $x$ = 0.0 and $x$ = 0.8 during redox reactions.The original hexagonal lattice (denoted by H1) was retained for $x$ in the range 0–0.25. In the range 0.25–0.55 for $x$, the redox reaction occurred only in the $M$ phase. At $x$ = 0.55, the $M$ phase was converted to a rhombohedral phase (denoted by H2), which proceeded in region for 0.55–0.75. A third rhombohedral phase (denoted H3) appeared at $x$ = 0.75. Similarly for NCA, three phase transitions occurred at 3.7, 4.0, and 4.2 $V$, which corresponded with the transitions of H1→M, M→H2, and H2→H3, respectively.

EIS, in Fig. 4, shows the charge-transfer resistance of 98, 200, 380, and 720 Ω for NCA-pristine, NCA-300, NCA-400, and NCA-500 respectively. The increase in charge-transfer resistance with heating temperature was due to the introduction of $Li_2MnO_3$ and deterioration of phase interface between NCA and electrolyte.

## Storage performance and pH

The storage performance of Ni-rich cathodes is also closely related to the surface properties. The test material was placed in petri dish at 25(±2)°C with humidity of 80%. As shown in Fig. 5, the weight gain for NCA-400 was significantly reduced, indicating improved storage performance. This can be attributed to the inhibition of reaction between cathode material and $H_2O/CO_2$ in air. The heat treatment of coating did not significantly change the total amount of lithium (Table 2). Simultaneously, the pH also dropped from 12.19 to 11.69. The pH did not change noticeably after 400 °C, indicating that the reaction between the residual LiOH in NCA and $MnCO_3$ was nearly complete at 400 °C.

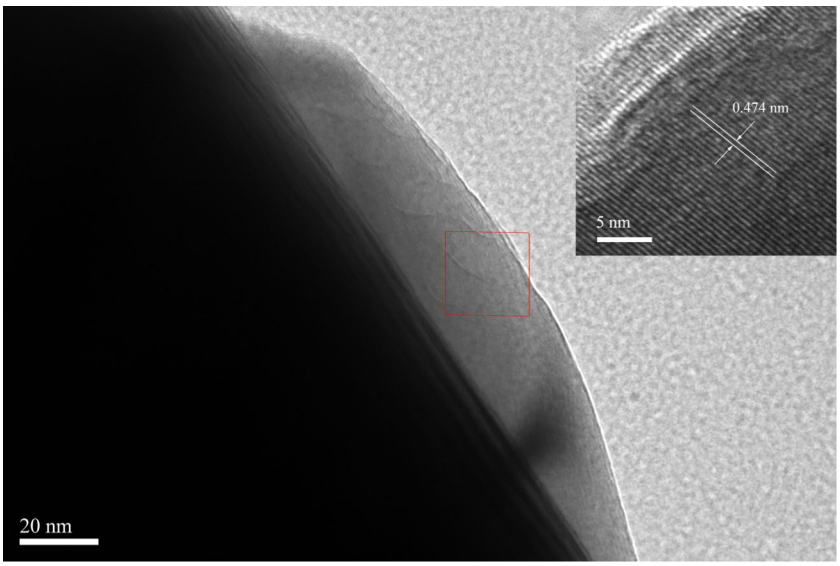


**Fig. 6** TEM image (inset, HRTEM image of red zone) for NCA-400

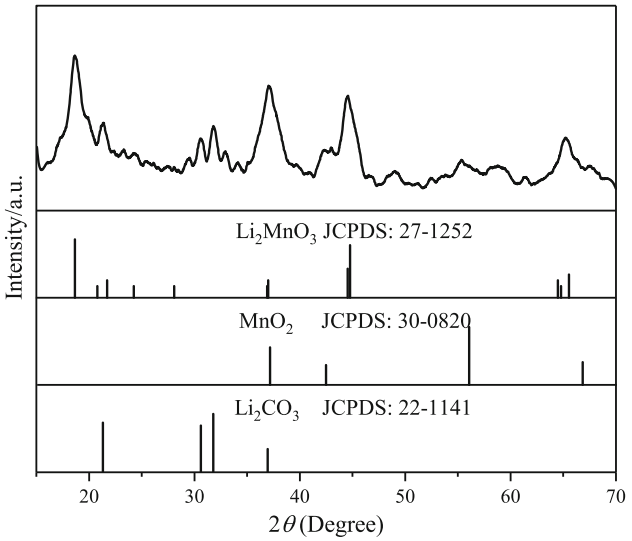


**Fig. 7** XRD patterns for the product of LiOH and $MnCO_3$ heated at 400 °C

## Evidence for formation of $Li_2MnO_3$

In order to confirm the formation of $Li_2MnO_3$ on the surface, the NCA-400 sample was analyzed by HRTEM. As shown in Fig. 6, a layer of about 20 nm was well coated on the surface of NCA-400. The inset HRTEM image shows the layered structure with a lattice spacing of 0.474 nm, which could be assigned to the (002) crystal facet of $Li_2MnO_3$. From this result, it is evident that the residual lithium on the surface was successfully converted to $Li_2MnO_3$ upon addition of $MnCO_3$.

For further verification, a mixture of LiOH and $MnCO_3$ (with 2:1 molar ratio) was heated at 400 °C in pure oxygen (99%). Figure 7 shows the corresponding XRD patterns. The peak at 18.6° clearly showed a layered structure. The reaction product contained $Li_2MnO_3$, $Li_2CO_3$, and $MnO_2$. The $Li_2CO_3$ was formed due to the generation of $CO_2$ by $MnCO_3$, which was also the reason for the decrease in pH. This result confirmed that $Li_2MnO_3$ was formed at 400 °C.

The distribution of Mn on the surface was examined by energy dispersive spectrometry (EDS). As shown in Fig. 8, Mn was uniformly distributed on the surface of secondary particle. As the result of the low heating temperature, most of the added Mn was distributed on the surface and not the core. Thus, the improved electrochemical performance was attributed to the surface coating of $Li_2MnO_3$.

## Thermal stability at delithiated states

The thermal stability of Ni-rich cathodes in delithiated states is an important factor to consider since it is closely related to the safety of lithium ion batteries. Figure 9a shows the weight loss during heating for $Li_{0.20}Ni_{0.80}Co_{0.15}Al_{0.05}O_2$. The 0.5% weight loss originated from the adsorbed $H_2O$ in cathode. Both samples showed the same onset decomposition temperature of 198 °C. Guilmard [28] has reported that $Li_{0.3}Ni_{1.02}O_2$ released oxygen at 190 °C. Furthermore, NCA-400 showed less weight loss between 198 and 350 °C, indicating that NCA-400 released less oxygen. Figure 9b also showed a higher peak temperature of 226 °C for NCA-400, compared to 221°C for NCA-pristine.

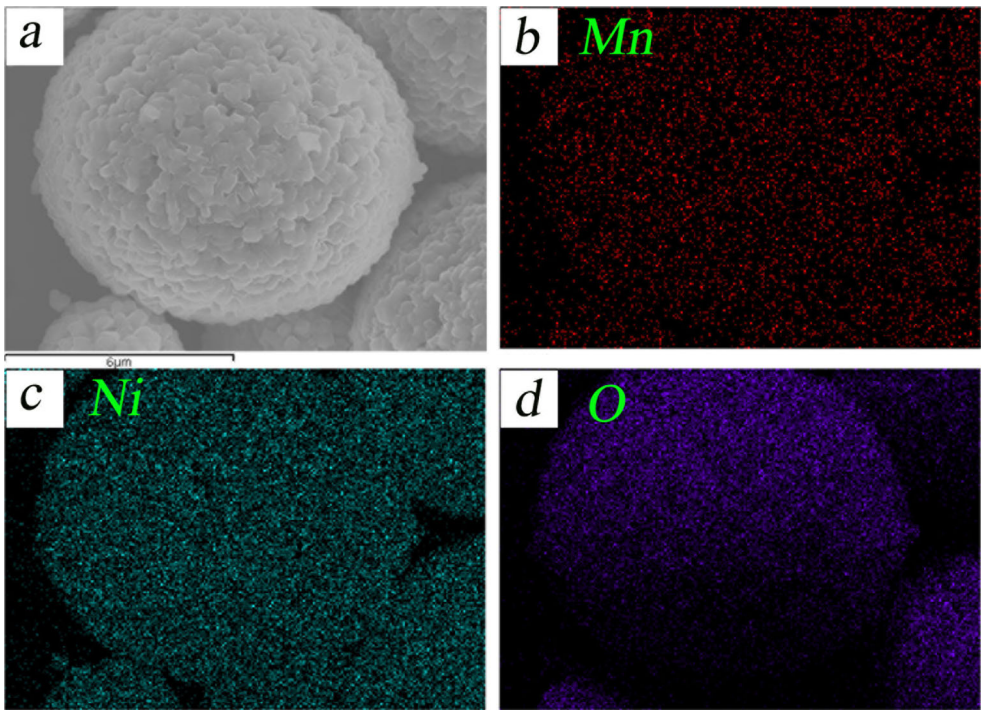


**Fig. 8** EDS mapping spectra on the surface of NCA-400

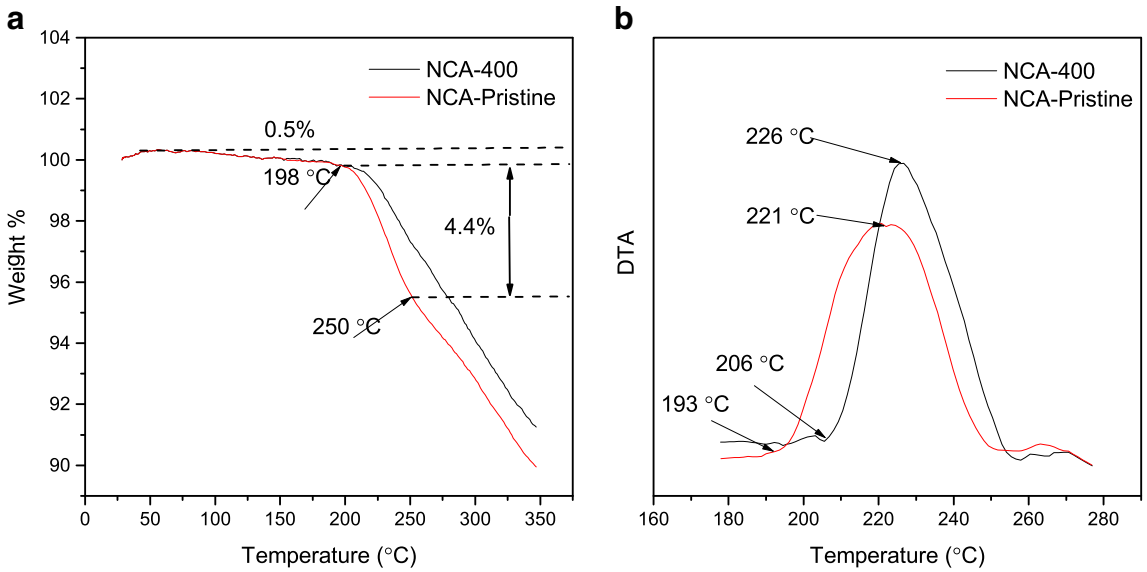


**Fig. 9** **a** TG and **b** DTA curves for NCA-pristine and NCA-400 after being charged to 4.3 V

These results confirmed the superior thermal stability for coated NCA.

## Conclusions

In this study, $Li_2MnO_3$-coated NCA cathode material was successfully prepared, which displayed high capacity and excellent capacity retention. In addition, the pH was also lowered at the same time. The improved cycle stability was attributed to the suppression of side reactions between cathode material and electrolyte. Hence, the dry-coat method using $MnCO_3$ to react with residual lithium was demonstrated to be an effective approach to improve the performance of Ni-rich cathode materials. Moreover, this method is economical for large-scale production.

**Funding information** This work was financially supported by the National Key R&D program of China (2016YFB0100500).



## References

1. Sasaki T, Nonaka T, Oka H, Okuda C, Itou Y, Kondo Y, Takeuchi Y, Ukyo Y, Tatsumi K, Muto S (2009) Capacity-fading mechanisms of $LiNiO_2$-based lithium-ion batteries. J Electrochem Soc 156:A289–A293
2. Kojima Y, Muto S, Tatsumi K, Kondo H, Oka H, Horibuchi K, Ukyo Y (2011) Degradation analysis of a Ni-based layered positive-electrode active material cycled at elevated temperatures studied by scanning transmission electron microscopy and electron energy-loss spectroscopy. J Power Sources 196:7721–7727
3. Watanabe S, Kinoshita M, Hosokawa T, Morigaki K, Nakura K (2014) Capacity fading of $LiAl_yNi_{1-x-y}Co_xO_2$ cathode for lithium-ion batteries during accelerated calendar and cycle life tests (effect of depth of discharge in charge-discharge cycling on the suppression of the micro-crack generation of $LiAl_yNi_{1-x-y}Co_xO_2$ particle). J Power Sources 260:50–56
4. Kleiner K, Melke J, Merz M, Jakes P, Nagel P (2015) Unraveling the degradation process of $LiNi_{0.8}Co_{0.15}Al_{0.05}O_2$ electrodes in commercial lithium ion batteries by electronic structure investigations. Acs Appl Mater Inter 7:19589–19600
5. Shizuka K, Kiyohara C, Shima K, Takeda Y (2007) Effect of $CO_2$ on layered $Li_{1+z}Ni_{1-x-y}Co_xM_yO_2$ (M = Al, Mn) cathode materials for lithium ion batteries. J Power Sources 166:233–238
6. Eom J, Kim MG, Cho J (2008) Storage characteristics of $LiNi_{0.8}Co_{0.1+x}Mn_{0.1-x}O_2$ (x = 0, 0.03, and 0.06) cathode materials for lithium batteries. J Electrochem Soc 155:A239–A245
7. Matsumoto K, Kuzuo R, Takeya K, Yamanaka A (1999) Effects of $CO_2$ in air on Li deintercalation from $LiNi_{1-x-y}Co_xAl_yO_2$. J Power Sources 81:558–561
8. Zhang XY, Jiang WJ, Zhu XP, Mauger A, Qilu JCM (2011) Aging of $LiNi_{1/3}Mn_{1/3}Co_{1/3}O_2$ cathode material upon exposure to $H_2O$. J Power Sources 196:5102–5108
9. Liu HS, Zhang ZR, Gong ZL, Yang Y (2004) Origin of deterioration for $LiNiO_2$ cathode material during storage in air. Electrochem Solid State Lett 7:A190–A193
10. Liu HS, Yang Y, Zhang JJ (2006) Investigation and improvement on the storage property of $LiNi_{0.8}Co_{0.2}O_2$ as a cathode material for lithium-ion batteries. J Power Sources 162:644–650
11. Moshtev R, Zlatilova P, Vasilev S, Bakalova I, Kozawa A (1999) Synthesis, XRD characterization and electrochemical performance of overlithiated $LiNiO_2$. J Power Sources 81:434–441
12. Park JH, Park JK, Lee JW (2016) Stability of $LiNi_{0.6}Mn_{0.2}Co_{0.2}O_2$ as a cathode material for lithium-ion batteries against air and moisture. B Korean Chem Soc 37:344–348
13. Xunhui X, Zhixing W, Peng Y, Huajun G, Fengxiang W, Jiexi W, Xinhai L (2013) Washing effects on electrochemical performance and storage characteristics of $LiNi_{0.8}Co_{0.1}Mn_{0.1}O_2$ as cathode material for lithium-ion batteries. J Power Sources 222:318–325
14. Kim J, Hong YS, Ryu KS, Kim MG, Cho J (2006) Washing effect of a $LiNi_{0.83}Co_{0.15}Al_{0.02}O_2$ cathode in water. Electrochem Solid State Lett 9:A19–A23

15. Naushad (ed) (2012) Life cycle assessment of wastewater treatment. Massachusetts Institute of Technology, Boston
16. Sulz CH (1888) A treatise on beverages or the complete practical bottler. Dick & Fitzgerald Publishers, New York
17. Kim H, Lee K, Kim S, Kim Y (2016) Fluorination of free lithium residues on the surface of lithium nickel cobalt aluminum oxide cathode materials for lithium ion batteries. Mater Design 100:175–179
18. Ring RJ, Royston D (1973) A review of fluorine cells and fluorine production facilities. Australian Atomic Energy Commission
19. Manthiram A, Knight JC, Myung ST, Oh SM, Sun YK (2016) Nickel-rich and lithium-rich layered oxide cathodes: progress and perspectives. Adv Energy Mater 6:1501010
20. Cho Y, Oh P, Cho J (2013) A new type of protective surface layer for high-capacity Ni-based cathode materials: nanoscaled surface pillaring layer. Nano Lett 13:1145–1152
21. Huang B, Li XH, Wang ZX, Guo HJ, Shen L, Wang J (2014) A comprehensive study on electrochemical performance of Mn-surface-modified $LiNi_{0.8}Co_{0.15}Al_{0.05}O_2$ synthesized by an in situ oxidizing-coating method. J Power Sources 252:200–207
22. Yang J, Xia YY (2016) Suppressing the phase transition of the layered Ni-rich oxide cathode during high-voltage cycling by introducing low-content $Li_2MnO_3$. Acs Appl Mater Inter 8:1297–1308
23. Zhang HL, Li B, Wang J, Wu BH, Fu T, Zhao JB (2016) Effects of $Li_2MnO_3$ coating on the high-voltage electrochemical performance and stability of Ni-rich layer cathode materials for lithium-ion batteries. Rsc Adv 6:22625–22632
24. Cao CH, Zhang J, Xie XH, Xia BJ (2017) Composition, structure, and performance of Ni-based cathodes in lithium ion batteries. Ionics 23:1337–1356
25. Jo JH, Jo CH, Yashiro H, Kim SJ, Myung ST (2016) Re-heating effect of Ni-rich cathode material on structure and electrochemical properties. J Power Sources 313:1–8
26. Jung SK, Gwon H, Hong J, Park KY, Seo DH, Kim H, Hyun J, Yang W, Kang K (2013) Understanding the degradation mechanisms of $LiNi_{0.5}Co_{0.2}Mn_{0.3}O_2$ cathode material in lithium ion batteries. Adv Energy Mater 1300787
27. Ohzuku T, Ueda A, Nagayama M (1993) Electrochemistry and structural chemistry of $LiNiO_2$ (R-3m) for 4 volt secondary lithium cells. J Electrochem Soc 140:1862–1870
28. Guilmard M, Croguennec L, Delmas C (2003) Thermal stability of lithium nickel oxide derivatives. Part II: $Li_xNi_{0.70}Co_{0.15}Al_{0.15}O_2$ and $Li_xNi_{0.90}Mn_{0.10}O_2$ ($x = 0.50$ and 0.30). Comparison with $Li_xNi_{1.02}O_2$ and $Li_xNi_{0.89}Al_{0.16}O_2$. Chem Mater 15:4484–4493